Shear alignments in three-dimensional simulations of lamellar phases

Peilong Chen
Department of Physics and Center for Complex Systems, National Central University, Chungli 320, Taiwan
(Received 15 October 2004; revised manuscript received 3 March 2005; published 17 June 2005)

Experiments studying layer orientation of sheared lamellar phases have consistently observed not only the seemingly obvious parallel orientation (with layers parallel to the shear plane), but also the so called perpendicular orientation (with layer normals along the vorticity direction) at the condition of higher shear frequencies and near the lamellar phase transition. We find that three-dimensional simulations of a deterministic mesoscopic dynamical equation (without thermal fluctuations) under the convection of simple shear flows have shown exactly such a dependence. The simulations show the important role played by the transverse orientation (layer normal along the velocity direction) and highlight the mechanism of the shear alignment being the competition between the shear frequency and the mesoscopic time scale of pattern organization.

DOI: 10.1103/PhysRevE.71.061503 PACS number(s): 83.10.Tv, 82.70.Uv, 83.50.Ax, 61.25.Hq

I. INTRODUCTION

Lamellar and smectic phases of many soft matter materials have many interesting and important properties [1]. When a sample is prepared in the condition of lamellar phases, such as lowering the system temperature below the transition point, usually it is seen to develop a characteristic length scale (e.g., as observed in scattering experiments) corresponding to the preferred layer spacing. However, the layers are usually poorly organized and do not show coherent lamellae in a macroscopic scale. Because the samples are usually in liquid states, among many possible external forces which could organize layers in large scales, shear flows are proved to be effective.

In addition to promoting uniform layers, experiments applying shears to lamellar phases have also revealed interesting alignments of the layers relative to the shear direction. In many different experiments using the thermotropic and lyotropic liquid crystals [2–4], block copolymers [5–12], liquid crystal polymers [13,14], and surfactants [15], there is a general characteristic for the appearance of two alignments under shear: the so called *C* orientation (Fig. 1), which has the layer normals along the shear velocity gradient direction, and the *A* orientation with the layer normals pointing in the vorticity direction. Although the *C* orientation is initially regarded as the obvious result, it was seen repeatedly that the *A* orientation appears at the condition near the lamellar transition and of high shear frequencies. At low shear frequencies or away from the lamellar phase transition point, the *C* orientation is obtained.

Recently an interesting molecule dynamics (MD) simulation [16] using amphiphilic dimer particles has investigated the transformation of the *B* orientation (with the layer normals along the velocity direction) to the *C* and *A* orientations under shear flows. Similarly, under high shears the transition to *A* alignments is seen, and to *C* alignments at low shears.

With the trend being seen in different materials (and even in the simple dimer MD simulations), it points to a universal mechanism independent of detailed material microscopic structures. However, the mechanism of such selection is still puzzling. Some researchers have argued that the crossover shear frequency above which the *A* orientations are obtained is related to a characteristic frequency associated with local domain deformation [10,11].

It is then reasonable to expect that the mechanism of alignment selections would be captured by a dynamical equation describing lamellar phases in a mesoscopic scale. In this paper we present results from three-dimensional simulations of such a deterministic dynamical model. Our results show shear-dependent alignments consistent with the general characteristics as seen in experiments. By studying the time evolutions of components in different orientations and observing their competitions, we find that the *B* orientation plays an important role. We identify two key mechanisms responsible for these shear induced alignments.

The first mechanism is that from an isotropic and poorly organized lamellar phase, kinetics of shear deformations actually promotes organization in both *A* and *B* alignments. The second is the competition at phase boundaries between the *A* orientation and *B*/*C* alignment (those intermediate between *B* and *C*, i.e., the layer normals on the velocity-velocity gradient plane). At low shear rates the *B*/*C* alignments are seen to expand into the *A* region, and opposite at high shears. The crossover shear rates are related to the characteristic inverse time scales of the pattern relaxation.

Our model is based on the well-known model *H* as classified in Ref. [17]. It is noted that we neglect both the hydrodynamics (the momentum equation) and fluctuations. Our results showing consistence with experiments without these two factors suggest that they are not important here. As will be discussed in more detail below, the dynamics seen in

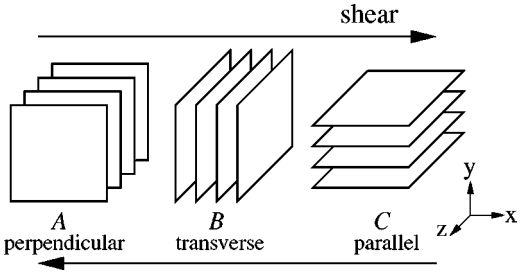

FIG. 1. Three principal orientations of layers with respect to the shear flow.

simulations leading to the shear alignment involve deterministic responses to the shear deformation. Some deviations introduced by the hydrodynamics should not change the main effects of shear deformation. Thus we would reason that it is not the deciding factor for the transition between *C* and *A* alignments. Furthermore the degree of deviation due to hydrodynamics will be highly dependent on the materials. The fact that the transition is universal in different materials suggests that the hydrodynamics might not be an important factor.

Similarly we have also neglected the fluctuation term from our model. While the fluctuation is an essential part of a thermodynamic description, we feel that it probably plays a minor role in our study concentrating on the diffusive relaxation of system structure driven by external shears.

While the oscillatory shears are commonly used in experiments, we have used both the oscillatory and steady shears in our simulations. They give essentially the same conclusions. There is only one parameter, the shear rate $\dot{\gamma}$, in steady shears, while the oscillatory shears have two parameters, the shear frequency ω and amplitude γ_m. However, the difference should not be significant because, with γ_m at order 1 (as chosen in most experiments), the oscillatory shears have similar average shear rates with the steady shears when $\omega \approx \dot{\gamma}$. Experiments [9,12] have also shown that the crossovers from the *C* to *A* orientations occur in the combination of $\gamma_m\omega$ in oscillatory shears.

It was often seen that the *A* orientation flips back to the *C* orientation at even higher shear frequencies larger than another characteristic frequency ω_c. In diblock copolymers, it is thought that ω_c is related to the conformation relaxation time scale of the polymer chains [11]. In polystyrene-polyisoprene melts, it is also argued that the flipping back to the *C* orientation at high shears is due to the mechanical contrast (difference in the viscoelastic response of the two blocks) [7,10,18]. Most experiments were performed near the glass transition point of PS, resulting in a stiffer PS block relative to the PI block. In a mixed surfactant-water (DMPC/$C_{12}E_5$/water) system [15], the flipping back from *A* to *C* is also seen at high shear rates. The experiments observe a 10% increase of the wavelength at the flip, hinting the possible changes of microscopic structures. The authors also speculated on the role of defect formation in this behavior.

Nevertheless these processes involving microscopic structures are beyond the simple generic mesoscopic model we consider in this paper. Effects of shear deformation on detailed microscopic dynamics, as postulated to be related to the flipping back to *C* orientation at high shears, can only be considered in detail models specific to different samples.

Previous theories [19] have been proposed that the shear alignments are due to the effects of shear flows on thermal fluctuations of layers in thermal equilibrium for well-aligned domains. In our model the thermal fluctuation is not included and the shear alignments are due to deterministic nonequilibrium dynamical processes. Although there seems no obvious reasoning to distinguish the two different modelings, we do believe that the dynamical approach, combined with numerical simulations, does offer many opportunities to model material properties and complex dynamics. Anyway, under shear a system is in principle in a nonequilibrium state. Some of the stability properties of uniform well-aligned lamellae have been studied [20].

Recently there are simulations of the model we used to study the shear alignment of the hexagonal cylinder phases [21]. They obtain at high shears the perpendicular hexagonal cylinders and the parallel ones at low shears. However, in our simulations we demonstrate that in the mechanisms leading to lamellar phase alignment, the formation and dynamics of the *B* (transverse) orientation play an important part. In the report of the cylinder phases, the selection mechanism between perpendicular and parallel has not been clarified and the significance of transverse cylinders is not seen.

II. THE MODEL AND SIMULATION METHODS

In the mesoscopic scale the system is described by an order parameter $\psi(\boldsymbol{r})$. The lamellar phases are formed by the distribution of regions of positive and negative ψ values. For example in a symmetric diblock copolymer melt, the two polymers have the same total volume fraction and, assuming incompressibility, the sum of the two local densities $\rho_1+\rho_2$ is a constant. The order parameter would be defined as $\psi \equiv \rho_1 - \rho_2/(\rho_1+\rho_2)$. Thus $\psi=1$ indicates a pure first-polymer phase and $\psi=-1$ for the second.

Dynamics of $\psi(\boldsymbol{r})$ is modeled to be driven by the relaxation of the free energy *F*, which is written as a functional of $\psi(\boldsymbol{r})$ [22],

$$F = \int \left(-\frac{1}{2}\psi^2 + \frac{1}{4}\psi^4 + \frac{1}{2}|\nabla \psi|^2 \right) d\boldsymbol{r} + \frac{1}{2}B \int\int \frac{\psi(\boldsymbol{r})\psi(\boldsymbol{r}')}{|\boldsymbol{r}-\boldsymbol{r}'|} d\boldsymbol{r}\, d\boldsymbol{r}'.$$

Here we have written the free energy in a dimensionless form. To model diblock copolymers, the original expression written in terms of the polymer parameters such as the degree of polymerization, the segment length, and the Flory-Huggins parameter can be found in Ref. [22]. When $B<\frac{1}{4}$ this free energy has a lamellar solution $\psi(\boldsymbol{r}) \sim \cos \boldsymbol{q}\cdot\boldsymbol{r}$ as the minimum free energy state with a constant finite $\boldsymbol{q}$. The time evolution of ψ, with the addition of the shear convection term, is then assumed to be

$$\frac{\partial \psi}{\partial t} + (\boldsymbol{v}_0 \cdot \boldsymbol{\nabla})\psi = \nabla^2 \frac{\delta F}{\delta \psi} = \nabla^2\left(-\psi + \psi^3 - \nabla^2\psi\right) - B\psi. \tag{1}$$

This equation is in the form of the well-known model *H* as classified in Ref. [17]. The random noise term is not included in the model. The flow $\boldsymbol{v}_0$ is taken as the simple shear flow field: $\boldsymbol{v}_0 = \dot{\gamma} y \hat{\boldsymbol{x}}$. (See Fig. 1.) The shear plane is on the *x*-*z* plane and the velocity is in the *x* direction. In principle there is also the momentum equation (hydrodynamics) which include the contributions from the osmotic pressure of ψ and the viscosity contrast of different phases. This could introduces deviations from the simple shear flow. In this paper we neglect the momentum equation and take the flow as a simple shear.

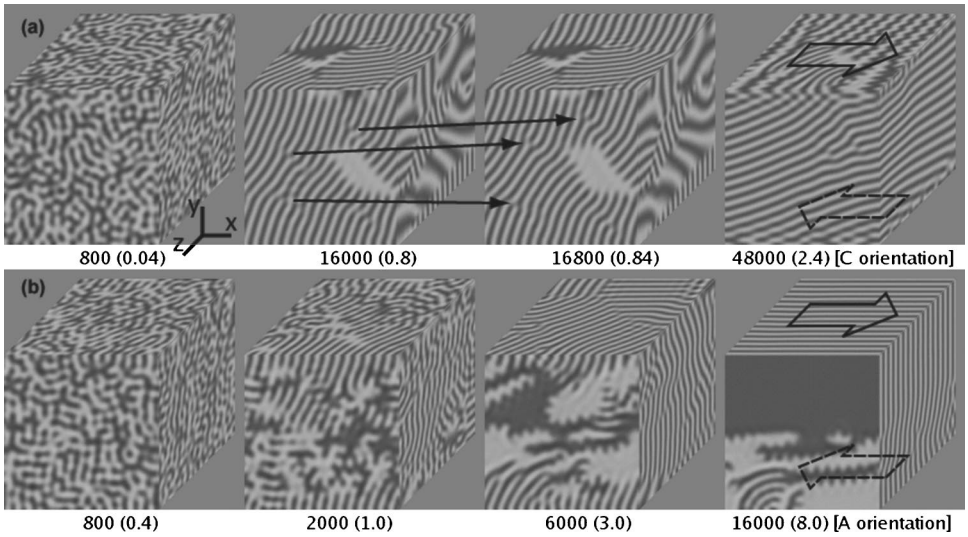

FIG. 2. Two examples of time evolutions of ψ under steady shear with time evolving from left to right. (a) $\epsilon=0.1$ and $\dot{\gamma}=0.000\,05$; (b) $\epsilon=0.1$ and $\dot{\gamma}=0.0005$. The numbers below each frame denote the time and shear strain (inside the parentheses). The shear flow direction is indicated by the two big arrows at the rightmost frames. The three arrows in the middle two frames of (a) are showing the motions of edge dislocations.

Without shear the lamellar phase transition is at $B_c=1/4$. With the reduced control parameter defined as $\epsilon\equiv(B_c-B)/B_c$, Eq. (1) gives lamellar solutions when $\epsilon>0$, with a critical wave number $q_c=\sqrt{1/2}$ at $\epsilon\to 0$. Thus ϵ plays a similar role of the quenched depth below the temperatures of, e.g., the order-disorder transition for diblock copolymers and the nematic-smectic transition for liquid crystals. Also, the time scale of the lamellar phase evolution is inversely correlated to ϵ.

There are three principal orientations of the lamellar phases relative to the shear flow. As illustrated in Fig. 1, lamellar phases with wave vectors in the x,y, and z directions are conventionally called the B,C, and A orientations, respectively. In the literature they are also referred to as the transverse, parallel, and perpendicular alignments, respectively. From Fig. 1 it is clear that the shears would continuously tilt and compress B (toward C) orientations while leaving uniform A and C alignments unchanged.

Three-dimensional simulations of Eq. (1) are done in rectangular boxes using a pseudospectral method [23]. In the x direction the periodic boundary condition is used. Since the imposed simple shear flow $\boldsymbol{v}_0=\dot{\gamma}y\hat{\boldsymbol{x}}$ is not compatible with the periodic boundary condition in the y direction, ψ is taken to have zero normal derivatives on the boundaries of the x-y and x-z planes.

Time evolutions of the simulations use the implicit method for the linear terms on the right hand side of Eq. (1). The convection and nonlinear terms are treated by the explicit Euler method [23].

III. RESULTS AND DISCUSSION

The selections of final alignments are studied by starting simulations from small random ψ fields under various values of the control parameter ϵ, with the application of steady or oscillatory shears. Two examples of simulations under steady shear are shown in Fig. 2. The results under oscillatory shear are essentially the same. The upper panel shows the time evolution at $\epsilon=0.1$ and $\dot{\gamma}=0.000\,05$. The two big arrows on the last graph depict the direction of the applied shear flow and the numbers below each graph indicate the time elapsed and the shear strain (inside the parentheses). (The shear strain values are defined as $\Delta y/\Delta x$.) The time evolution shows that the system develops a final C (parallel) alignment. On the other hand in the lower panel, the shear rate is increased to $\dot{\gamma}=0.0005$. It is seen that a final A (perpendicular) alignment is instead formed.

The final alignments depending on the shear rate (frequency) and ϵ are shown in Fig. 3 for the steady shears and for the oscillatory shears with a 2.0 maximum shear amplitude in Fig. 4. The solid squares denote the A orientations and the open ones the C. It is expected that the B orientations will not be stable since they are tilted continuously by the shear. In both figures, the distinction between the A and C orientations is that the A orientations occupy the region of high shear rates (frequencies) and are near the order-disorder transition (small ϵ). The crossover shear rates (frequencies) separating the two orientations increase with ϵ.

In Figs. 3 and 4, some squares have the upper parts of their interiors filled to different proportions. They indicate that the simulations yield the A or C orientations from dif-

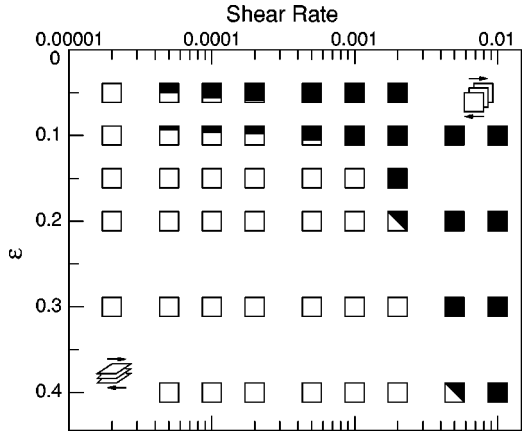

FIG. 3. The appearance of the A (the solid squares) and C (the open squares) orientations under the steady shears at different values of the shear rate $\dot{\gamma}$ and control parameter ϵ. See text for explanations about the two kinds of half-filled squares.

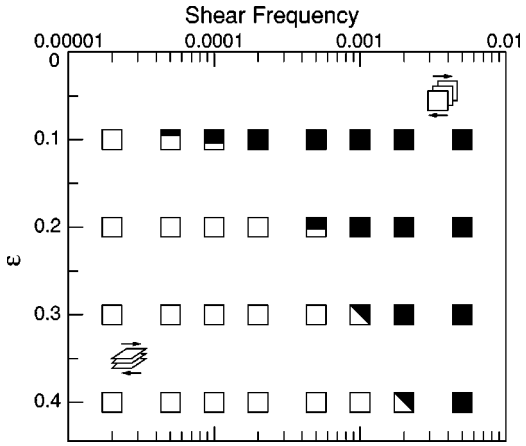

FIG. 4. The appearance of the A (the solid squares) and C (the open squares) orientations under the oscillatory shears (with a maximum shear strain of 2.0) at different values of the shear frequency ω and control parameter ϵ. See text for explanations about the two kinds of half-filled squares.

ferent small random initial distributions. The reason that the system does not always evolve to a definite final state is probably due to the finite size of the simulation box. Nevertheless after many simulations (on the order of 25) at each condition, we count the occurrence of the A and C orientations. The proportional area filled inside each square is proportional to the fraction of appearance of the A orientation. We can see that this fraction is consistent with the trend of the C to A transition at high shear rates (frequencies).

Also there are squares with filled triangles, especially near the C-A transition at higher shear rates (frequencies). They indicate final lamellar states with no dependence on the flow velocity direction ($\hat{x}$): $\psi=\psi(y,z)$. Their dynamics essentially become two dimensional with the flow no longer playing any role. Typically they are irregular lamellar distributions on the y-z plane and further evolution is very slow.

This selection diagram shows shear alignments similar to those found in many experiments, for example in liquid crystal polymers of the main-chain BB-5(3-Me) polyester [14]. This also occurs in a lyotropic lamellar phase of the mixed DMPC/$C_{12}E_5$/water system [15]. (Interestingly the transition to the smectic phase was obtained by increasing temperature.)

For diblock copolymers, experiments using (ethylene-propylene)-poly(ethylethylene) samples [5,6] have also shown similar behaviors. Nevertheless there are some disagreements for polystyrene-polyisoprene (PS-PI) samples [7–9,12], where at lower shear rates two experiments found A orientations and two others found C orientations. The results were summarized in Ref. [10]. They identified a frequency ω_d which they suggested characterizes an inverse time of local domain deformation. The experimental results were summarized as follows: at $\dot{\gamma}<\omega_d$, two A and two C orientations are seen in four studies and at $\dot{\gamma}>\omega_d$ all studies see A orientations.

Another paper [11] which also measured the A(high shear)-C(low shear) behavior in PS-PI suggested that the explanation for the preference of the A alignment is related to

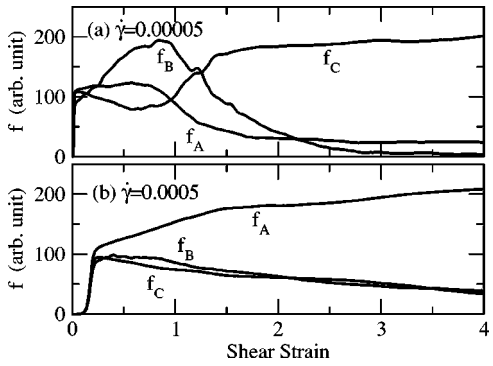

FIG. 5. Time evolutions of the f's (corresponding to Fig. 2) at $\epsilon=0.1$ with $\dot{\gamma}=(a)$ 0.0005; (b) 0.000 05.

the theories proposed earlier [19] that layer fluctuations of the lamellae are coupled to the shear in the parallel (C) orientation, making it less favorable than the perpendicular (A) alignment. Since the shear needs to be faster enough to be effective such that the fluctuations are not averaged out, it is the A alignments to be expected at high shear rates.

However, without fluctuations and concerning mainly the dynamical relaxation, our simulations show different mechanisms leading to the shear alignment. Because in our model dynamics is driven by free energy relaxation toward coherent layer structures, we propose that the important rate ω_d is the rate for lamellae organizing toward coherent layers. The control parameter ϵ serves as an indication of the time scale about the evolution of domain structures and the lamellar organization (larger $\epsilon\rightarrow$ faster organization). So ω_d should be roughly proportional to ϵ. In both Figs. 3 and 4 we see that the transition shear rates and frequencies increase with ϵ. This supports the idea that the competition between the ω_d and shear rate (frequency) determines the selection of the A and C orientations.

To understand the detailed mechanisms leading to the C to A transition, we want to consider the temporal evolution of system wave vectors. To characterize the orientation of a mixed lamellar phase we simply define f_B as

$$f_B = \sum_{q_x>q_y,q_x>q_z} |\psi(\boldsymbol{q})|^2$$

and similarly for f_C (with $q_y>q_x$, $q_y>q_z$) and f_A (with $q_z>q_x$, $q_z>q_y$). Thus f_B, f_C, and f_A quantify the relative magnitudes of the B, C, and A orientations, respectively.

In Fig. 5, time evolutions of the f's from the simulations shown in Fig. 2 are shown. In Fig. 5(b), initially from a state with a small random field of ψ, all f's quickly reach a similar value ($\sim$100 in the figure) corresponding to an isotropic lamellar state. Evolution of this isotropic state shows that f_A gradually increases under the action of the shear with both f_B and f_C decreasing, indicating that the shear deformation is promoting uniform distribution of ψ on the velocity-velocity gradient plane.

When $\dot{\gamma}$ is decreased to 0.000 05 in Fig. 5(a), we see a different and interesting evolution. Although the final state is

the C orientation, after the initial growth for all f's we find that both f_A and f_B components increase when f_C decreases. f_A and f_B reach maximum values roughly at the shear strain 0.8, with f_B larger than f_A. If we examine the second frame of Fig. 2(a) we can see that it is indeed showing the development of dominating B orientation under shear flows. The shear then gradually tilts the B toward C, also manifested in Fig. 5(a) in which f_B and f_A start to decline and at the same time f_C begins to increase and eventually dominates.

The time evolutions in Fig. 5 seem to suggest two mechanisms involved in forming the A alignments at high shears. First the shear kinetics enhance the A and B alignments initially. Second, at high shears the A orientation is winning the competition against the B/C orientation and losing at low shears.

The first mechanism in which the shear initially enhances the A and B alignments should relate to the nature of shear, which produces deformation in the x-y plane. Consider the shear driving a continuous shear deformation on the x-y plane in an isotropic lamellar state. We can envision that the free energy relaxation, responding to the deformation of $\psi(\mathbf{r})$, would promote homogeneity of $\psi(\mathbf{r})$ on the x-y or y-z plane, but not the x-z plane. For example when two separate blobs of the same phase on a particular x-y plane are brought together by shear convection, they will merge and enhance uniformity on the x-y or y-z plane, depending on circumstance, but never on the x-z plane. Together with the effect of shear also tilting and compressing the layers in the B orientation, we could understand that while in Fig. 5(a) both the A and B components increase, it is only A that increases in Fig. 5(b) at high shears.

We also remark that at $\dot{\gamma} \leqslant 0.000\,02$ for the steady shear and $\omega \leqslant 0.000\,02$ for the oscillatory shear, sometimes we did obtain a tilted B-C orientation (depending on initial conditions). This probably is another indication of the shear enhanced B orientation. Such states are still tilted by the shear flows. Because the shear rates are very low, the layers have enough time to uniformly break on a particular x-z plane and reconnect to relieve the tilting angle. This of course may just be an artifact due to the limited size of the simulation box. However, it is noted that there were observations of the B or B/C orientations under oscillatory shears in experiments using various samples of diblock copolymers [24].

We also discuss briefly the process of the B to C conversion, which can be seen in Fig. 2(a). The production and motion of edge dislocations [25] play essential roles. As the layers are tilted and compressed, they merge to create edge dislocations. Motions of the edge dislocations then relieve the compression. Three arrows are drawn in Fig. 2(a) to indicate these dislocation motions. The layers can thus maintain the original wavelength and gradually tilt toward the C alignment.

From Fig. 5, the other mechanism leading to high shear A alignment involves the competition between different orientations. To probe this mechanism we study the time evolutions from initial conditions consisting of two regions with well-aligned orientations. As Fig. 5(a) suggests the initial growth of both A and B orientations under shear, we look at the time evolutions of prepared initial distributions consisting of mixed A and B alignments as shown in Figs. 6 and 7.

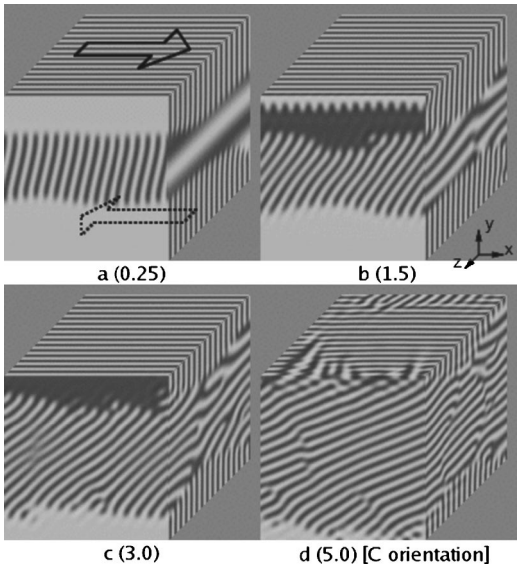

FIG. 6. Time evolution at $\epsilon=0.2$ and $\dot{\gamma}=0.0005$ with a mixed A-B initial condition under a steady shear. The B orientation in the central part gradually expands as time evolves from (a) to (d). The number below each frame indicates the shear strain. The two big arrows show the shear flow direction.

With $\epsilon=0.2$, the time evolution at $\dot{\gamma}=0.0005$ as in Fig. 6 shows that the B alignment at the central region gradually expands, while at $\dot{\gamma}=0.002$ as in Fig. 7 the B region shrinks and then disappears. This characteristic is consistent with the final alignment summarized in Fig. 3 after we recognize that the B alignment is eventually converted into C.

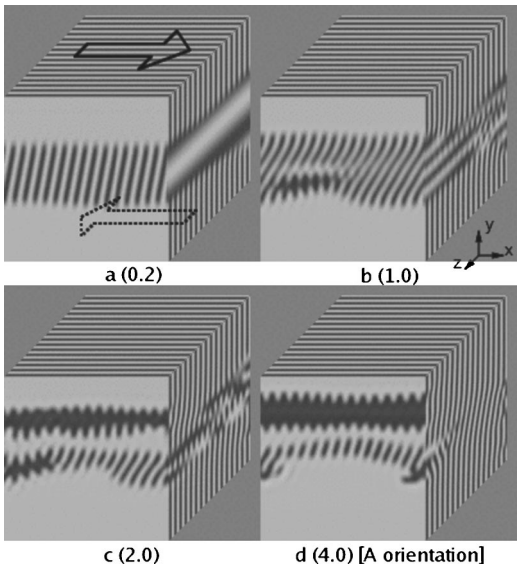

FIG. 7. Time evolution at $\epsilon=0.2$ and $\dot{\gamma}=0.002$ with a mixed A-B initial condition under a steady shear. The B orientation in the central region gradually shrinks and disappears as time evolves from (a) to (d). The number below each frame indicates the shear strain. The two big arrows show the shear flow direction.

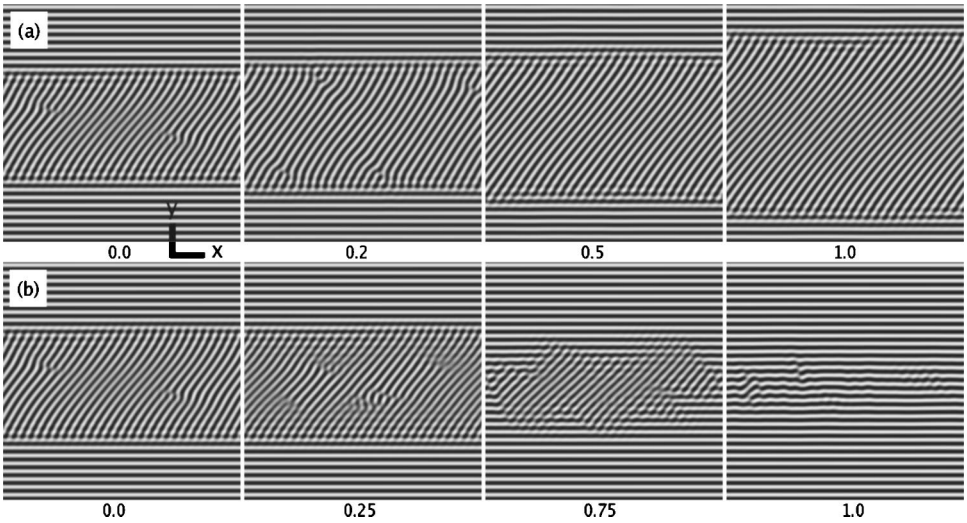

FIG. 8. Time evolution with a mixed *B*-*C* initial condition. (a) $\epsilon = 0.2$ and $\dot{\gamma} = 0.000\,05$. The *B* orientation in the central region maintains the tilting angle and gradually expands as time evolves from left to right. (b) $\epsilon = 0.2$ and $\dot{\gamma} = 0.0002$. The *B* orientation in the central part gradually shrinks and disappears as time evolves. The numbers indicate the shear strain.

So while the central *B* layers are tilted continuously by the shear, the responses depend crucially on $\dot{\gamma}$. Similar behaviors as those shown in Figs. 6 and 7 are also seen when the *A* orientations are replaced by *C* in the initial distributions. These time evolutions are shown as two-dimensional simulations in Fig. 8.

For both mixed *A*-*B* and *B*-*C* distributions, as the shear tilts the *B* orientations, its effective wavelength decreases, causing the increase of free energy. However, at low shear rates these tilted stripes actually maintain their tilting angles and relieve the compression by expanding vertically toward the *A* or *C* region, as seen in Figs. 6 and 8(a). This mechanism can be clearly seen in Fig. 8(a) where the tilting angle of the *B* region remains unchanged under the action of steady shear. Thus the tilting action of the low applied shear on the *B* orientation actually drives its expansion.

With the increased shear rate, the *B* expansion whose speed is dictated by the control parameter ϵ cannot follow the shear. The layers cannot maintain a constant tilting angle and the wavelength is decreasing with increasing tilting angle [as clearly seen in the middle two frames of Fig. 8(b)]. With the compressed layers not favored by the free energy relaxation, the system then relaxes by shrinking the region of the *B* orientation.

When we start simulations from an initial distribution of a uniform *B* orientation, we see evolutions very similar to those discussed above. (1) At small shear rates, the tilted and compressed layers nucleate dislocations to relieve compression, similar to those seen in Fig. 2(a). The lamellae gradually convert to the *C* orientation with defect nucleation and motion. (2) At large shear rates, it seems that there is not enough time for the defects to form and the *B* orientation essentially melts under shear compression. Then incoherent lamellae first form and they quickly align to the *A* orientation with the action of shear.

Finally we note that if the simulations are started from perfect lamellae of the *C* orientation, application of a shear larger than the transition value will not convert them to the *A* alignment. Similarly, the *A* orientation does not transform to the *C* under a small shear. However, uniform *C* and *A* lamellae are prepared artificially in the finite simulation size, which is strongly limited by computation ability. In real experimental samples, one understands that a state identified by, e.g., the scattering data as the *C* or *A* orientations will still contain many imperfections. The competition between different orientations as seen in our simulations then has a very good chance to induce transitions under shear.

IV. CONCLUSION

The appearance of the *A* and *C* orientations in sheared lamellar phases in many experiments using different materials has shown consistent characteristics such that the *A* orientation appears at the condition of high shear rates and close to lamellar phase transition points. In this paper from three-dimensional simulations we show that a mesoscopic dynamical equation displays a shear alignment of the lamellar phases very similar to those found in experiments. Two key mechanisms are seen in simulations leading to the formation of the *C* orientation at low shear rates (frequencies) and the *A* in high shears. The first is that with a random lamellar distribution, shear deformations enhance both *A* and *B* orientations initially. The second mechanism is that low shears actually drive the expansion of tilted *B* orientations but high shears have the opposite effect. It is shown that the reason for expanding *B* orientations is that the expansion can relieve the layer compression induced by the shear flow. In conclusion the response of the *B* (transverse) lamellae to the shear is the crucial element determining the final alignment.

For the future we believe that three-dimensional simulations of the mesoscopic model can be very useful in the study of complex phase dynamics in soft matter systems. Especially with the increase of computational ability, we can undertake simulations with (1) a larger system size, (2) the inclusion of the fluctuation terms, and (3) the consideration of the momentum equation with adequate modeling of the material viscoelastic properties. It is hoped that interesting dynamics will be found with such studies.

ACKNOWLEDGMENT

This work is supported by the National Science Council of Taiwan.

[1] I. W. Hamley, *Introduction to Soft Matter* (John Wiley & Sons, Chichester, 2000).
[2] C. R. Safinya, E. B. Sirota, R. R. Bruinsma, C. Jeppesen, R. J. Plano, and L. J. Wenzel, Science **261**, 588 (1993).
[3] P. Panizza, P. Archambault, and D. Roux, J. Phys. II **5**, 303 (1995).
[4] J. Berghausen, J. Zipfel, P. Lindner, and W. Richtering, Europhys. Lett. **43**, 683 (1998);J. Zipfel, P. Lindner, M. Tsianou, P. Alexandridis, and W. Richtering, Langmuir **15**, 2599 (1999).
[5] K. Koppi, M. Tirrell, F. Bates, K. Almdal, and R. Colby, J. Phys. II **2**, 1941 (1992).
[6] K. A. Koppi, M. Tirrell, and F. S. Bates, Phys. Rev. Lett. **70**, 1449 (1993).
[7] S. Patel, R. Larson, K. Winey, and H. Watanabe, Macromolecules, **28**, 4313 (1995).
[8] V. Gupta, R. Krishnamoorti, J. Kornfield, and S. Smith, Macromolecules, **28**, 4464 (1995).
[9] D. Maring and U. Wiesner, Macromolecules **30**, 660 (1997).
[10] T. Tepe, D. Hajduk, M. Hillmyer, P. Weimann, M. Tirrell, F. Bates, K. Almdal, and K. Mortensen, J. Rheol. **41**, 1147 (1997).
[11] Z. R. Chen, J. A. Kornfield, S. D. Smith, J. T. Grothaus, and M. M. Satkowski, Science **277**, 1248 (1997).
[12] H. Leist, D. Maring, T. Thurn-Albrecht, and U. Wiesner, J. Chem. Phys. **110**, 8225 (1999).
[13] L. Noirez, Phys. Rev. Lett. **84**, 2164 (2000).
[14] M. Tokita, K. Tokunaga, S. Funaoka, K. Osada, and J. Watanabe, Macromolecules **37**, 2527 (2004).
[15] O. Dhez, F. Nallet, and O. Diat, Europhys. Lett. **55**, 821 (2001).
[16] H. Guo, K. Kremer, and T. Soddemann, Phys. Rev. E **66**, 061503 (2002).
[17] P. C. Hohenberg and B. I. Halperin, Rev. Mod. Phys. **49**, 435 (1997).
[18] Y. Zhang and U. Wiesner, J. Chem. Phys. **103**, 4784 (1995).
[19] M. E. Cates and S. T. Milner, Phys. Rev. Lett. **62**, 1856 (1989);G. H. Fredrickson, J. Rheol. **38**, 1045 (1994);M. Goulian and S. T. Milner, Phys. Rev. Lett. **74**, 1775 (1995).
[20] F. Drolet, P. Chen, and J. Viñals, Macromolecules **32**, 8603 (1999);P. Chen and J. Viñals, *ibid.* **35**, 4183 (2002).
[21] K. Luo and Y. Yang, Polymer **45**, 6745 (2004).
[22] H. Kodama and M. Doi, Macromolecules **29**, 2652 (1996).
[23] See, e.g., C. Canuto, M. Hussaini, A. Quarteroni, and T. Zang, *Spectral Methods in Fluid Dynamics* (Springer-Verlag, Berlin, 1988).
[24] S. Okamoto, K. Saijo, and T. Hashimoto, Macromolecules **27**, 5547 (1994);Y. Zhang and U. Wiesner, J. Chem. Phys. **103**, 4784 (1995);B. S. Pinheiro, D. A. Hajduk, S. M. Gruner, and K. I. Winey, Macromolecules **29**, 1482 (1996).
[25] L. D. Landau and E. M. Lifshitz, *Theory of Elasticity* 3rd ed. (Butterworth-Heinemann, Oxford, 1995).